Available online at www.sciencedirect.com

ScienceDirect

Procedia Structural Integrity 2 (2016) 1724–1737

Structural Integrity Procedia

www.elsevier.com/locate/procedia

21st European Conference on Fracture, ECF21, 20-24 June 2016, Catania, Italy

The use of SE(T) specimen fracture toughness for FFS assessment of defects in low constraint conditions

J.-J. Han[a], N.O. Larrosa[b,*], R.A. Ainsworth[c], Y.-J. Kim[a]

[a]*Department of Mechanical Engineering, Korea University, Anam-Dong, Seongbuk-Gu Seoul 136-701, Korea.*
[b]*School of Materials, The University of Manchester, Manchester M13 9PL, United Kingdom*
[c]*School of Mechanical, Aerospace & Civil Engineering, The University of Manchester, Manchester M13 9PL, United Kingdom.*

Abstract

Due to the loss of constraint, shallow cracked specimens can 'absorb' more energy than deeply cracked specimens commonly used to define the critical value to fracture and therefore exhibit a higher fracture toughness. The increase in energy absorption allows a reduction in the inherent conservatism when assessing components in low constraint conditions. This study addresses the benefit of using shallow cracked SE(T) fracture toughness specimens in fitness for service (FFS) assessment of defects under low constraint conditions, e.g. blunt defects or shallow cracks. Tearing resistance curves (J-R curves) have been constructed by means of a virtual test framework to determine crack initiation and propagation for shallow cracked SE(T) specimens and parametric notched C(T) specimens. The effect of constraint level on J-R curves is compared. It is observed that most of the blunted C(T) specimens analysed exhibit the same or a lower toughness value than that of a shallow cracked SE(T) specimen. The results are used to show how reduced conservatism can be made in defect assessment of blunt defects or in cases in which reduced constraint conditions can be demonstrated.

Keywords: Apparent fracture toughness, Constraint effect, Shallow defects, Blunt defects, *J-R* curves, Stress-modified fracture strain model, Structural integrity

1. Introduction

Structural integrity assessment procedures for components containing flaws, e.g. cracks, usually evaluate fitness-for-service (FFS) by means of Engineering Critical Assessments (ECA). ECA is based on damage tolerance principles (fracture mechanics) and is used to assess whether or not a defective component is in a safe condition from elastic-plastic fracture and plastic collapse under specified loading and environmental conditions. For elastic-plastic fracture, the driving force is quantified by a single parameter (K, CTOD or J-integral), and compared with the respective critical value to failure, usually obtained from testing standard laboratory specimens. In standard fracture toughness testing, such as ASTM E399 (2005) and ASTM E1820 (2006), deeply cracked compact tension, C(T), or single edge notch

* Corresponding author. Tel: +44 (0)161 306 4286.
E-mail address: nicolas.larrosa@manchester.ac.uk

10.1016/j.prostr.2016.06.218

bend, SE(B), specimens are typically used to ensure plane strain conditions and high in-plane constraint conditions at the crack tip. This leads to a toughness value measured from standard laboratory specimens which is a lower bound value to that relevant to conditions in a defective component. In some cases this may lead to an exaggerated underestimation of the material capacity to withstand load. This is done to avoid measurement of fracture toughness values specific to every structural geometry, loading and crack size of interest.

Crack-tip stress fields can be divided into hydrostatic and shear components. Yielding of the material is governed by the shear component of the stress field. Tensile hydrostatic stresses contribute directly to the crack-tip opening mode but do not influence yielding. It follows, therefore, that fracture toughness is directly influenced by the hydrostatic component (σ_m) of the crack-tip stress field. Most engineering components are subjected to lower hydrostatic stresses than those in deeply cracked test specimens and benefit could be claimed by the development of an approach to account for the increase of load bearing capacity.

The inability of the single-parameter fracture mechanics to incorporate the change of fracture toughness with changes in specimen geometry and remote loading has been reported by McMeeking and Parks (1979) and Shih and German (1981). Effort has been aimed to extend the ability of fracture mechanics approaches to deal with crack tip constraint variations and approaches based on two-parameter descriptions of the crack-tip fields have been widely proposed, where K, J or CTOD characterizes the near-tip deformation field and the second parameter characterizes the level of stress triaxiality (hydrostatic stresses) over distances comparable to a few CTODs, as reported by Betegon and Hancock (1991) and O'Dowd and Shih (1991).

An alternative framework for constraint analysis and effective fracture toughness assessment is the application of failure models, often referred to as local approaches. Local approaches couple the loading history (stress-strain) near the crack-tip region with micro-structural features of the fracture mechanisms involved. Since the fracture event is described locally, the mechanical factors affecting fracture are included in the predictions of the model. The parameters depend only on the material and not on the geometry, and this leads to better transferability from specimens to structures than one- and two-parameter fracture mechanics methods. The benefits and drawbacks of both local approaches and two parameter fracture mechanics has been thoroughly discussed by Pineau (2006) and Ruggieri and Dodds (1996).

In this work, highly ductile materials are addressed for which ductile tearing is considered to be the principal mechanism for fracture. Resistance to crack growth is an important concept for damage tolerance assessments of structural integrity. A useful tool to assess ductile crack growth resistance is the J resistance curves or J-R curve. This curve represents the material's fracture toughness change with crack extension and is considered to be a material property.

A phenomenological model [Bao and Wierzbicki (2004) and Bao (2005)] based on a stress modified fracture strains concept is used to predict J-R curves [Kim et al. (2013)] and compare the results of a parametric analysis of notched compact tension C(T) with single edge tension SE(T) specimens for four different materials having different fracture criteria and tensile properties. Effective fracture toughness values are obtained from the J-R curves and the applied J representing the notch driving force is derived to characterize the crack tip stress fields. The approach presented in this study has been compared with J-R curves derived from load-load line displacement data according to ASTM E1820 (2006), with the results of both methods being in good agreement.

Although the phenomenological model is thoroughly discussed in several publications by Kim et al. (2004) and Oh et al. (2007, 2011), Section 2 briefly introduces the fundamental concepts of the model, the virtual testing technique and summarises the material properties of the materials under analysis. The different geometries of notched C(T) and the shallow cracked SE(T) specimen and FE analysis details are described in Section 3. Results and a comparison of the results for both types of specimens are presented and discussed in Section 4. The benefits of using the SE(T) fracture toughness in FFS assessments of components containing blunt defects are also discussed and quantified by means on reserve factors relative to those based on data from sharp cracked C(T) specimen. The work is concluded in Section 5.

2. Ductile fracture simulation model

Mechanistic ductile fracture models need to accurately describe the distinct mechanisms that occur in the process of ductile fracture (i.e., nucleation, growth and coalescence of voids), and involve the quantification of a large number

of micro-mechanical parameters from experimental measurements. The model implemented in this work, however, simplifies several of these mechanisms by taking advantage of some phenomenological observations. It is based on the concept of stress modified fracture strain previously applied by Bao and Wierzbicki (2004),Bao (2005),Kim et al. (2004),Oh et al. (2007) and Oh et al. (2011). As previously discussed by McClintock (1968),Rice and Tracey (1969) and Hancock and Mackenzie (1976), it has been demonstrated that true fracture strain for ductile materials is strongly dependent on the level of stress triaxiality. The model used in this study also establishes an exponential relationship between the true fracture strain and stress triaxiality (Fig. 1):

$$\epsilon_f = \alpha \ \exp\left(-\gamma \frac{\sigma_m}{\sigma_e}\right) + \beta \tag{1}$$

where α, β and γ are material constants obtained by fitting experimental data from smooth and notched bar tensile tests, Fig. 1 Oh et al. (2011), and

$$\frac{\sigma_m}{\sigma_e} = \frac{\sigma_1 + \sigma_2 + \sigma_3}{3\sigma_e} \tag{2}$$

where σ_i (i=1-3) are principal stresses and σ_e is the von Mises stress.

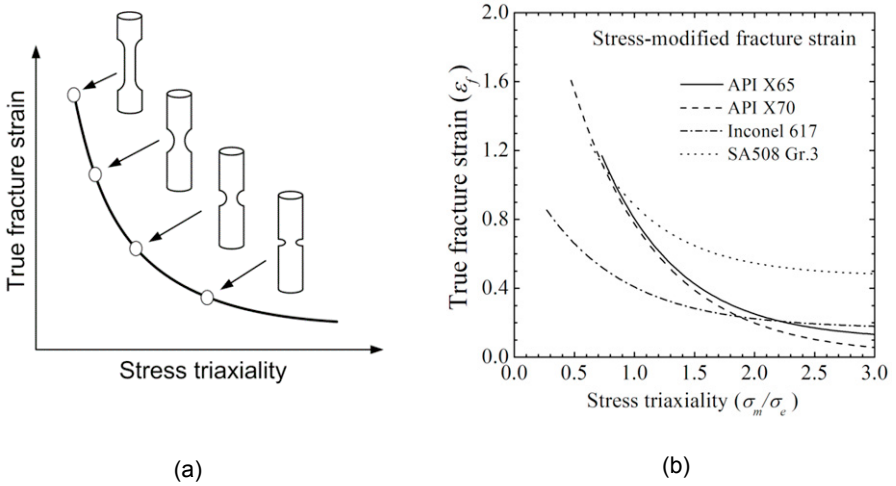

Fig. 1. (a) Phenomenological stress-modified fracture strain criterion and (b) Stress-modified fracture strain for the different materials, Oh et al. (2011); Kim et al. (2011); Jeon et al. (2013)

Using a finite element technique, this model is implemented in a step-by-step procedure in which at each loading step, the damage produced by incremental strain, $\Delta\omega$, is assessed and added to the total damage, ω, produced on previous steps. The quantification of the incremental damage definition is performed at each finite element of the model as follows:

$$\begin{aligned} \Delta\omega_i &= \frac{\Delta\epsilon_e^p}{\epsilon_f} \\ \omega_i &= \omega_{i-1} + \Delta\omega_i \end{aligned} \tag{3}$$

where $\Delta\epsilon_e^p$ is the equivalent plastic strain increment and ϵ_f is determined by the local triaxiality in the element. When the total damage becomes equal to unity (ω=1), local failure is assumed to occur at the element and the initiation and propagation of a crack is simulated by reducing all the stress components to zero, or at least to a sufficiently small value to make the contribution of the element to the resistance of the component negligible. For more details on the numerical implementation of the model, the reader is referred to the work of Oh et al. (2011).

3. Parametric Finite Element Analysis

Shallow cracked SE(T) and notched C(T) specimens were modelled by means of 3-D finite elements. Geometry dimensions and schematics of the specimens are shown in Fig. 2. API X65 and X70 pipeline steels, Inconel alloy 617, and SA508 grade 3 low alloy steel were considered to include the effect of different tensile and fracture behaviour properties. C(T) specimens with varying notch tip radius were analysed, to study the effect of constraint level variations on the fracture resistance of the specimen. This leads to what is usually referred as notch or effective fracture toughness, also discussed, -among others- by Spink et al. (1973), Milne et al. (1979),Horn and Sherry (2010) and Han et al. (2015) . Figure 3 shows 3-D FE models used in the ductile fracture simulations. Due to symmetry conditions

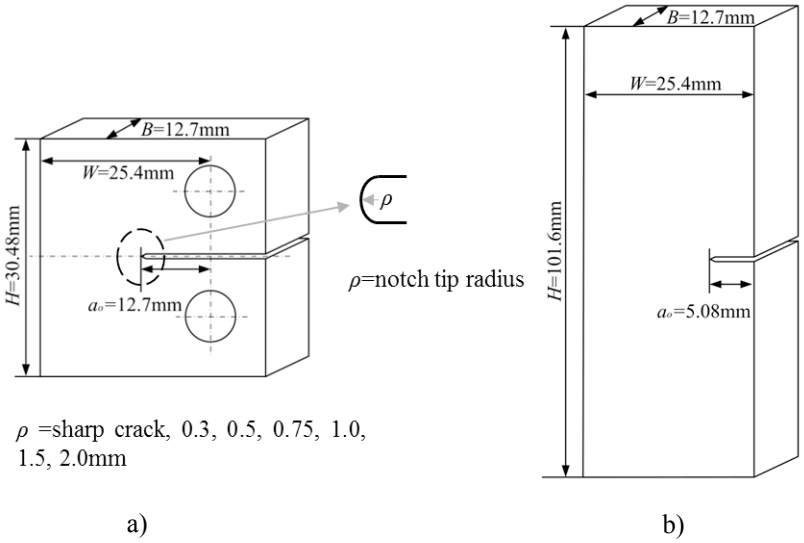

Fig. 2. Schematic illustration of fracture toughness specimens showing the dimensions: (a) Notched compact tension C(T) specimen ; (b) Single Edge Notch Tension SE(T) specimen

of load and geometry, a quarter of each specimen was modelled, to improve computational efficiency. It has been shown in the work by Oh et al. (2011) that the damage accumulation process is element-size dependent and therefore, element size should be determined based on calibration process with Eq. (1). The calibration of the FE mesh size is performed by means of comparison with experimental test results. The element size and the values of the material constants used in this work are shown in Table 1. A notch radius value equal to the calibrated mesh size is regarded as a sharp crack.

Table 1. Element size and constants defining the fracture criterion for each material

Material	Element Size (mm)	α	β	γ
API X65, Oh et al. (2011)	0.15	3.29	-1.54	0.01
API X70, Kim et al. (2011)	0.1	3.10	-1.4	0.01
INCONEL 617, Kim et al. (2011)	0.25	1.01	-1.43	0.17
SA 508, Jeon et al. (2013)	0.1	2.24	-1.68	0.47

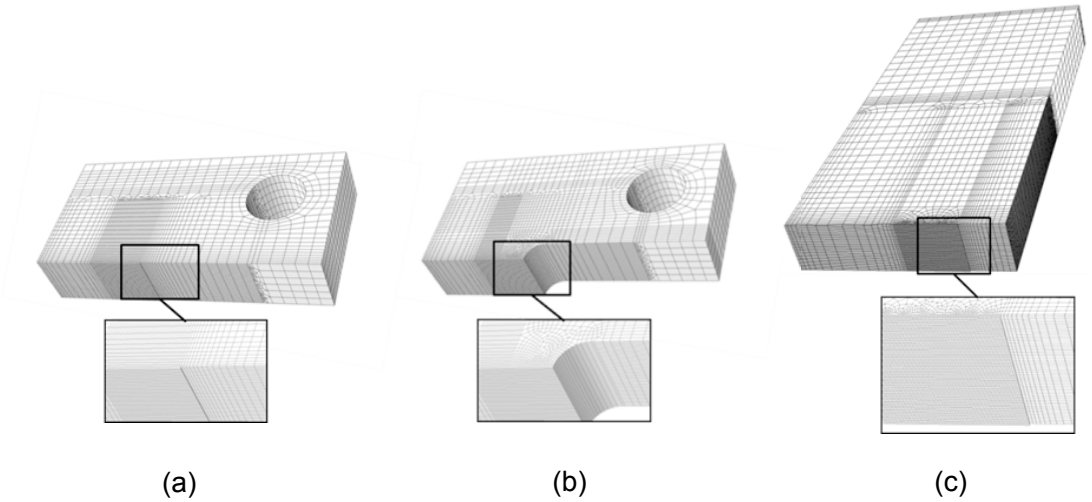

Fig. 3. Finite element models for API X65: (a) C(T), sharp crack, (b) C(T), ρ=2.0 mm and (c) SE(T), sharp crack

It should be noted that the local approach and the simulation procedure summarised above was verified by comparison with experimental data on fracture toughness test specimens and pressurised pipes with gouges, which can be regarded as the blunt defects considered in this work, and serves as validation for this purpose. For details on the validation of this approache please refer to the work by Kim et al. (2013), Kim et al. (2004), Oh et al. (2007, 2011).

For the SE(T) specimen, a fixed-grip loading condition was applied to the surface of the specimen producing a uniform displacement while for the C(T) specimens a displacement boundary condition was applied to a load pin and controlled by a reference node which was coupled with surface nodes of the pin hole using the MPC (multi-point constraint) option within ABAQUS. The total numbers of elements/nodes in the FE models range from 23,366/26,016 to 88,929/95,542..

To allow for the large geometry changes, the large geometry change option was chosen in the analyses. The damage model was implemented in ABAQUS by means of UHARD and USDFLD subroutines. Subroutine USDFLD is an auxiliary subroutine which is used to define or re-define field variables and to pass information, i.e. hydrostatic stress and equivalent stresses/strains at Gauss points, into the UHARD subroutine. In the UHARD subroutine, accumulated damage is calculated according to Eq. 3. When the accumulated damage becomes critical (ω=1), load-carrying capacity of the element is dissipated by changing the yield surface. For further details on the FE implementation of the damage model, the reader is referred to the work by Oh et al. (2011).

By applying the present approach, *J-R* curves were predicted using the domain integral method, as discussed by Parks (1977) and Shih et al. (1986), where the crack extension, δa, was obtained by using the nine-point average method recommended in ASTM E1820 (2006) . The integration domains were chosen to be sufficiently far away from the crack/notch tip to include the whole stress fields produced by the presence of the crack/notch but close enough to avoid any errors resulting from the influence of specimen boundaries. The values of J were extracted from each section of the specimens as shown in Fig. 4c and Fig. 4-1c, and averaged through the specimen thickness. This method has been verified in studies by Kim et al. (2004) and Oh et al. (2007, 2011) and by comparing ASTM standards and test results.

When the domain integral method is used for evaluating the J-integral, care should be taken to ensure that far-field J values match the values that would be obtained from experimental data, as reported by Brocks and Yuan (1989) and Yuan and Brocks (1991). A convergence analysis of the J-integral values for the different contours used was first performed to set the correct domains for accurate calculations, as presented in Fig. 4.

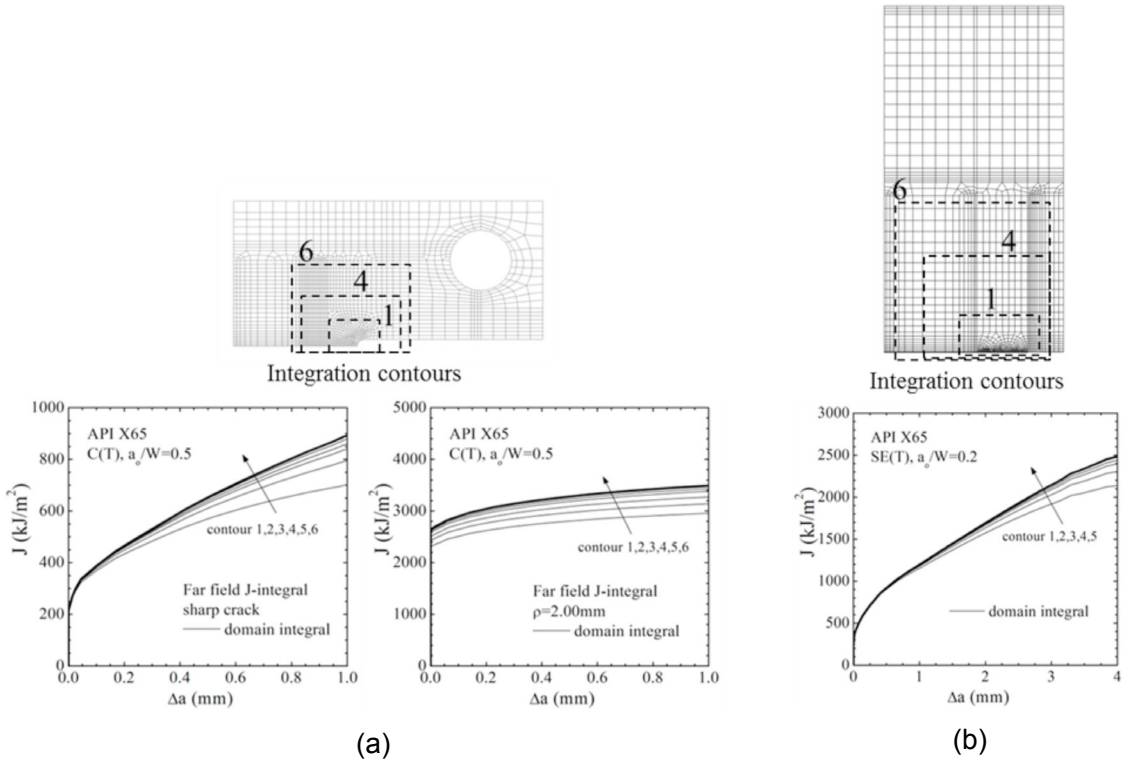

Fig. 4. *J-R* curves predictions for API X65 material, illustrating convergence analysis of domain integral values: (a) C(T) specimen, sharp crack and ρ=2.0mm ; (b) SE(T) specimen, sharp crack

4. Results

Numerical $J-R$ curves for the different specimens and the application of ESI (1992) procedure for the estimation of the effective fracture toughness are reported in this section. The dependence of the results on the notch bluntness and loading conditions is presented.

4.1. Non-sharp initial defects

The effect of notch bluntness and associated loss of constraint on the fracture behaviour of four different materials has been investigated by means of finite element (FE) analysis by Han et al. (2015). A summary of the results obtained by these authors is shown below as it is relevant to the analysis in the present work. Standard C(T) and notched C(T) specimens, Fig. 2a), of four different materials: API X65 and X70 pipeline steels, Inconel alloy 617, and SA508 Gr.3 low alloy steel were studied. As notch bluntness increases, it was found that the effective fracture toughness increased due to a less severe state of stress. Figure 5a presents J-R curves obtained from virtual testing method used in this study, and shows that the initiation toughness ($J_{0.2}$=J_{IC}) is increased when the notch radius increases. Figure 6 shows the normalised value of the notch initiation toughness for each material. As shown in the figure, a linear trend is observed in the normalised value of the notch fracture toughness with notch tip radius (ρ -J^{ρ}_{IC}/J_{IC}). The following equations were derived for the assessment of the apparent fracture toughness of the four different materials as a function of the

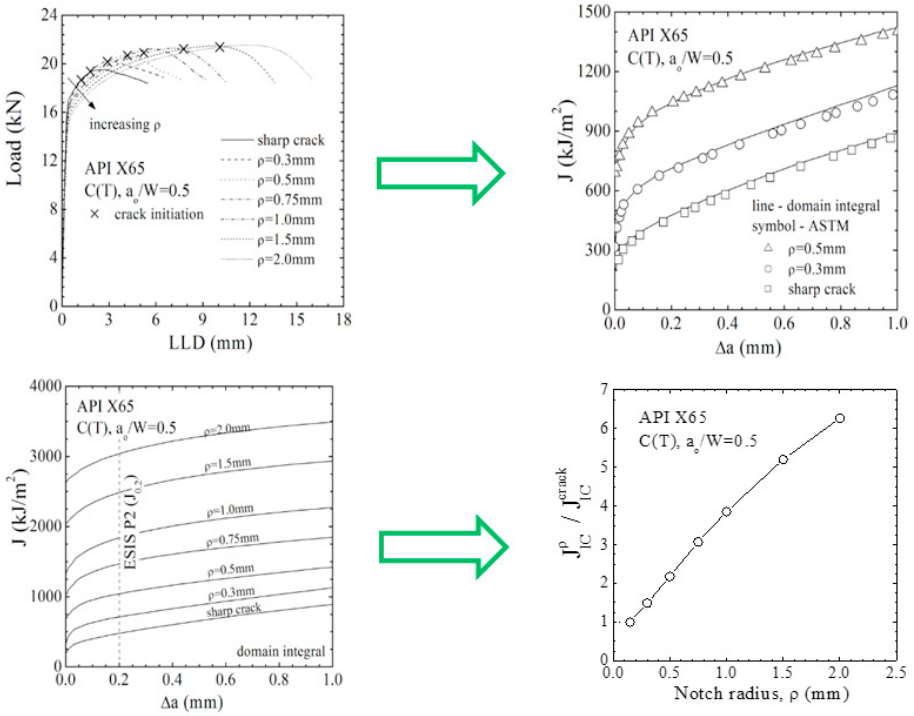

Fig. 5. Notch C(T) specimens: effect of radius on tearing resistance curve and fracture toughness (API X65).

notch tip radius, ρ (with 0.2 mm$\leq \rho \leq$2 mm):

$$\begin{aligned} J^{\rho}_{IC}/J_{IC} &= 5.342\rho + 0.306 && \text{(APIX70)} \\ J^{\rho}_{IC}/J_{IC} &= 2.890\rho + 0.734 && \text{(APIX65)} \\ J^{\rho}_{IC}/J_{IC} &= 2.576\rho + 0.710 && \text{(INCONEL617)} \\ J^{\rho}_{IC}/J_{IC} &= 2.828\rho + 0.734 && \text{(SA508Gr.3)} \end{aligned} \tag{4}$$

Results from the analysis led to the following outcomes:

- Fracture resistance curves ($J-R$ curves) predicted with the ductile fracture model shows excellent agreement with curves derived from load-load line displacement data according to ASTM E1820-13e1 (Figure 5)
- It was shown that increasing notch root radius (i.e. blunting the notch), led to an increase in the effective fracture toughness at both ductile initiation (defined at an engineering definition of 0.2mm of crack growth) and the subsequent resistance to ductile tearing (the J-R curve)
- These observations led to an increase in reserve factor when accounted for in a FFS assessment using the FAD. As expected, a blunt notch shows lessened likelihood of crack-dominated failure than a sharp crack. . It is also observed that the effective fracture toughness linearly increases with notch radius (Figure 6 and Equations 4).
- It was shown that the Option 1 Failure Assessment Diagram (FAD), developed for sharp cracks and used in most FFS codes, is also relevant to blunt notched C(T) specimens (Figure 7.a).
- The approach presented here may be applied with the FAD method to define a notch radius above which analysis may be based simply on plastic collapse, without the need to consider ductile fracture initiation (see Figure 7.b)
- The degree of conservatism in assuming a blunt defect as sharp was quantified by a reserve factor on the fracture parameter K_r, used in FAD methods and the results showed that the reserve factors could be increased by up to

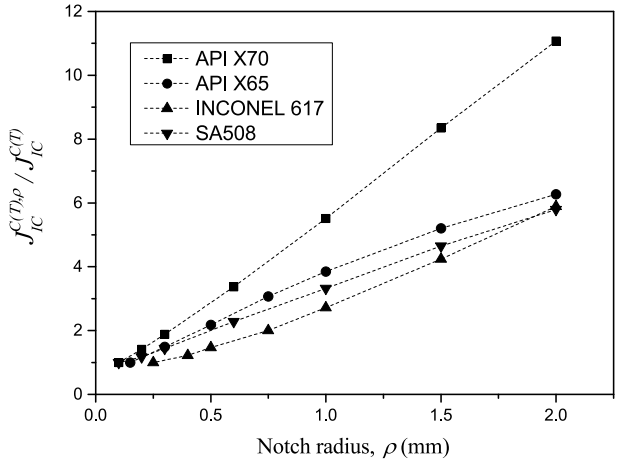

Fig. 6. Normalised initiation toughness of notched C(T) specimens for API X70 and API X65 pipeline steels, Inconel alloy 617, and SA508 Gr.3 low alloy steel

a factor of 3 greater for notched specimens relative to reserve factors for specimens with sharp cracks (Figure 7.c)

4.2. Constraint effect on fracture properties

The benefit of using the higher fracture toughness measured on shallow cracked single edge tension (SE(T)) specimens in FFS assessments is addressed here. Ductile fracture simulations performed by Han et al. (2015) are extended here to include shallow cracked SE(T) geometries. Again, *J-R* curves were constructed and a comparison of the stress fields ahead of the notch tip is reported, to specifically investigate the constraint effect in ductile fracture.

Figure 8 compares the stress triaxiality fields in the vicinity of sharp cracks and blunt notched C(T) specimens with that of a shallow crack SE(T) specimen. It is observed that in a SE(T) specimen the stress triaxiality is smaller and therefore the fracture-toughness value is expected to be higher than that in a high-constraint configuration such as the standard C(T) specimen.

Fracture resistance curves for both sharp crack SE(T) and C(T) specimens are shown in fig. 9. From the constructed *J-R* curves, the fracture toughness, J_{IC}, defined as the *J*-integral value at a crack extension of 0.2 mm was determined according to ESI (1992). Table 2 shows the values of J_{IC} for the different specimens and the value $J_{IC}^{SE(T)}/J_{IC}^{C(T)}$, quantifying the enhanced toughness of the shallow cracked SE(T) sample with respect to deeply cracked specimen.

Table 2. Predictions of initiation toughness: SE(T) VS. C(T). Values in kJ/m^2.

Material	$J_{IC}^{SE(T)}$	$J_{IC}^{C(T)}$	$J_{IC}^{SE(T)}/J_{IC}^{C(T)}$
API X65	655.89	475.85	1.378
API X70	392.00	292.74	1.339
INCONEL 617	546.77	475.62	1.149
SA 508	603.48	529.87	1.138

Analysis of Figs. 8 and 9 reveals an evident loss of constraint in the SE(T) specimen resulting in an increased capacity for sustaining load. For example, in most of the materials address in this work, the apparent fracture toughness for deeply cracked notch C(T) specimens with $\rho \geq 0.2$ mm, is greater than that of the shallow cracked SE(T) specimen ($J_{IC}^{C(T),\rho\geq 0.2\ mm} \geq J_{IC}^{SE(T)}$), showing that a standard C(T) specimen with more than 0.2mm notch radius is less

detrimental than a crack in a shallow cracked SE(T)(see Table 3). More importantly, $J_{IC}^{SE(T)}$ may be used to reduce over-conservatism (while still being conservative) when assessing structural integrity of components experiencing this level of stress triaxiality, instead of using $J_{IC}^{C(T)}$. This has been recently studied by Larrosa and Ainsworth (2016).

Table 3. Normalised initiation toughness: Notched C(T) vs SE(T). $J_{IC}^{C(T),\rho}/J_{IC}^{SE(T)} \geq 1$ shows conservatism when using $J_{IC}^{SE(T)}$ to assess a deep blunt defect.

API X70		API X65		INCONEL 617		SA508	
ρ (mm)	$\frac{J_{IC}^{C(T),\rho}}{J_{IC}^{SE(T)}}$	ρ (mm)	$\frac{J_{IC}^{C(T),\rho}}{J_{IC}^{SE(T)}}$	ρ (mm)	$\frac{J_{IC}^{C(T),\rho}}{J_{IC}^{SE(T)}}$	ρ (mm)	$\frac{J_{IC}^{C(T),\rho}}{J_{IC}^{SE(T)}}$
Crack	0.75	Crack	0.73	Crack	0.87	Crack	0.88
0.20	1.05	0.30	1.08	0.40	1.06	0.20	1.03
0.30	1.40	0.50	1.58	0.50	1.28	0.30	1.27
0.60	2.52	0.75	2.23	0.75	1.74	0.60	2.00
1.00	4.12	1.00	2.79	1.00	2.37	1.00	2.92
1.50	6.24	1.50	3.77	1.50	3.69	1.50	4.09
2.00	8.27	2.00	4.55	2.00	5.13	2.00	5.09

The numerical investigation using the local approach to fracture for the analysis of shallow crack components produced the following outcomes:

- A notched or shallow cracked specimen shows reduced crack tip constraint which reduces much more rapidly with load than a deeply cracked structure (Figure 8).
- The value of the applied J for a given load increases with decreasing notch acuity, that is, the crack driving force for a blunt defect is higher than that for a sharper one at a given load. This does not mean that a blunt notch is more detrimental than a sharp notch. There is a competition between the loss of constraint for the blunt notch, which would lead to an increase in the load carrying capacity, and the reduced limit load for a blunt notch, which leads to increased plasticity for a given load and a reduction in load carrying capacity.
- The increase in energy absorption (Figure 9) allows a reduction in the inherent conservatism when evaluating specimens in low constraint conditions.
- Notched C(T) specimens of ρ =0.2-0.3 mm have the same level of constraint as a shallow SE(T) specimen. This finding can have important implications for the assessment of blunt defects.
- It should be noted that this analysis has been performed for uniaxial Mode I loading only. It would be expected that positive biaxial loading conditions would act to restore some of the crack-tip constraint loss and reduce some of the fracture-toughness elevation associated with shallow flaws. This would require further study for components in which loading is primarily biaxial. However, biaxial loading also has a major influence on the load carrying capacity through an influence on the limit load, as reported by Meek and Ainsworth (2014, 2015).

5. Concluding remarks

The purpose of this study was to determine and quantify the influence of constraint conditions on the effective fracture toughness of different geometrical configurations of test specimens of four different materials: API X65 and X70 pipeline steels, Inconel alloy 617, and SA508 Gr.3 low alloy steel. The work byHan et al. (2015), on the notch bluntness effect on the apparent fracture toughness of notched C(T) specimens, has been extended to the analysis of a shallow cracked SE(T) specimen using the concept of stress-modified fracture strain.

Parametric studies were performed, where the effects of the geometric parameters ρ and a_0/W were considered. Fracture resistance curves, $J-R$ curves, were constructed by using the domain integral method and the stress fields ahead of the notch tip were reported, where the influence of the constraint conditions given by ρ and a_0/W were highlighted.

The parametric studies provide useful information on cases in which it may be possible to use the SE(T) fracture toughness to reduce conservatism in structural integrity assessments. The use of the SE(T) resistance curve as a material property in fracture assessments is recommended when the crack tip constraint conditions in the component

under consideration are comparable to those in the SE(T) specimen as recently studied by Larrosa and Ainsworth (2016). This reduces the conservatism of using the standard fracture toughness obtained from deeply cracked C(T) specimens.

Lower constraint conditions than that of deeply cracked standard C(T) specimens are found in blunted crack tips and shallow cracked specimens. From these results and those in the previous work by Han et al. (2015), it is evident that the local geometry (notch tip radius) and the crack depth affects the level of constraint at the crack tip and have a strong influence on the effective fracture toughness. The application of the shallow cracked SE(T) fracture toughness value in FFS assessment could have significant economic benefits, by reducing the current overly conservative approaches whilst maintaining structural integrity, defining margins on failure and indicating when plastic collapse is the dominant failure mechanism.

Acknowledgments

The authors would like to acknowledge the part funding and technical support from BP through the BP International Centre for Advanced Materials (BP-ICAM) which made this research possible. Useful discussions with Prof. Jae-Hoon Kim of Chungnam National University and Dr. Nak-Hyun Kim of Korea Atomic Energy Research Institute (KAERI) are greatly acknowledged.

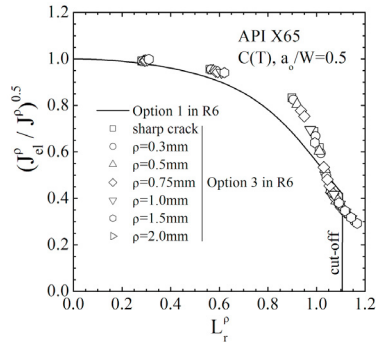

a) R6 Option 1 vs R6 Option 3

b) Effect of using $J_{IC}^{C(T),\rho}$ on assessment point

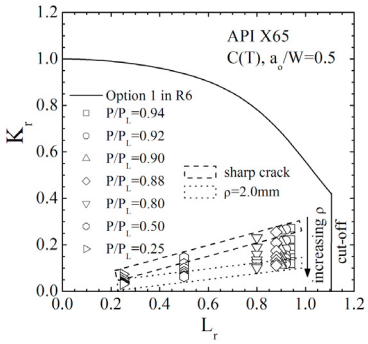

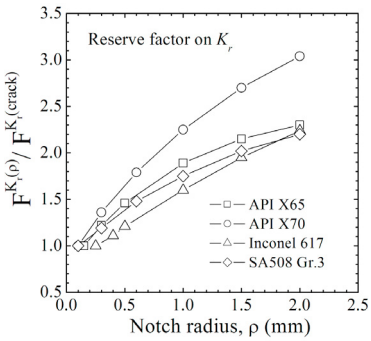

c) Reserve factors for the different materials

Fig. 7. Application to Structural integrity assessment within FAD framework.

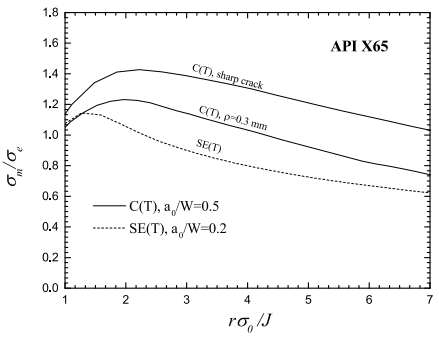

(a) API X65

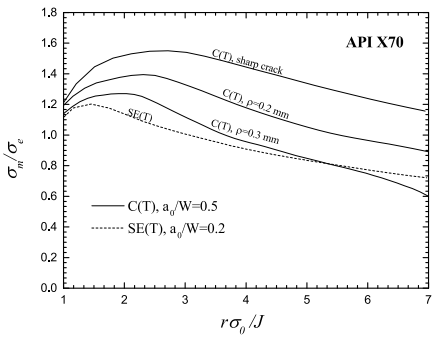

(b) API X70

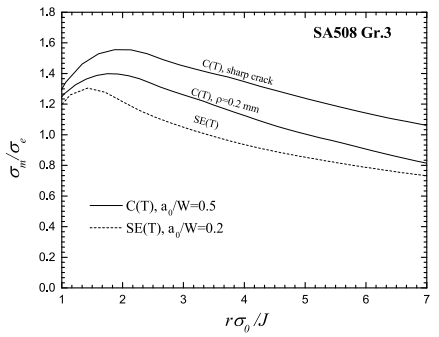

(c) SA 508 Gr.3

Fig. 8. Comparison of SE(T) and notched C(T) crack tip stress fields.

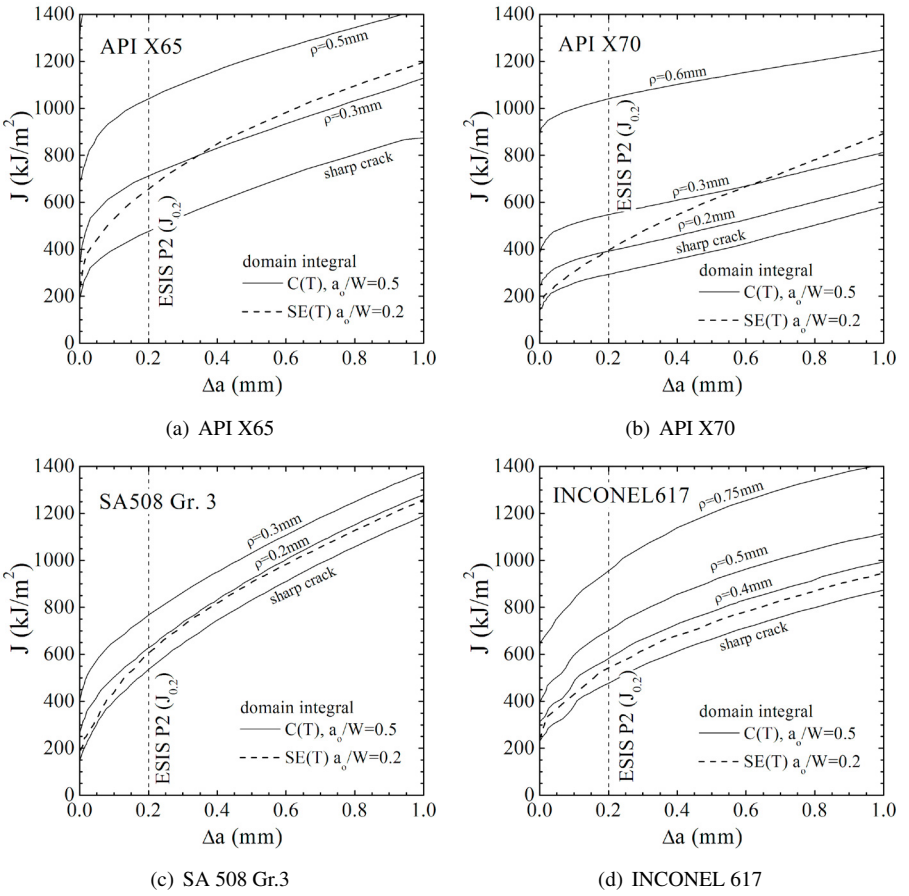

(a) API X65 (b) API X70

(c) SA 508 Gr.3 (d) INCONEL 617

Fig. 9. Fracture resistance curves of shallow crack SE(T) and deeply cracked C(T) specimens

References

ASTM E399-05, 2005. American Society for Testing and Materials. Standard Test Method for Plane-Strain Fracture Toughness of Metallic Materials .

ESIS P2-92, 1992. ESIS Procedure for Determining the Fracture Behaviour of Materials .

ASTM E1820-06A, 2006. American Society for Testing and Materials. Standard Test Method for Measurement of Fracture Toughness .

Anderson T., 1995. Fracture Mechanics: Fundamentals and Applications. CRC press, Taylor & Francis, Boca Raton, Florida, USA

Bao Y., 2005. Dependence of ductile crack formation in tensile tests on stress triaxiality, stress and strain ratios. Engineering Fracture Mechanics, 72, 505–522.

Bao Y., Wierzbicki T., 2004. On fracture locus in the equivalent strain and stress triaxiality space. International Journal of Mechanical Sciences 46, 81–98.

Betegon C., Hancock J.W., 1991. Two-parameter characterization of elastic-plastic crack-tip fields. Journal of Applied Mechanics, Transactions ASME 58, 104–110.

Brocks W., Yuan H., 1989. Numerical investigations on the significance of J for large stable crack growth. Engineering Fracture Mechanics 32, 459–468.

Han J.J., Larrosa N.O., Kim Y.J., Ainsworth R.A., 2016. Blunt defect assessment in the framework of the failure assessment diagram. International Journal of Pressure Vessels and Piping (submitted) .

Hancock J., Mackenzie A., 1976. On the mechanisms of ductile failure in high-strength steels subjected to multi-axial stress-states. Journal of the Mechanics and Physics of Solids 24, 147–160.

Horn A., Sherry A., 2010. Prediction of cleavage fracture from non-sharp defects using the Weibull stress based toughness scaling model. International Journal of Pressure Vessels and Piping 87, 670–680.

Jeon J.Y., Kim N.H., Kim Y.J., Lee S.Y., Kim J.W., 2013. Predictions of mechanical properties from small punch test results using FE damage analyses. American Society of Mechanical Engineers, Pressure Vessels and Piping Division , volume 1 A.

Kim J.H., Han J.J., Kim Y.J., Shim D.J., 2013. Comparison of J resistance curves from toughness testing specimens with those from various cracked pipe tests. American Society of Mechanical Engineers, Pressure Vessels and Piping Division , volume 6 A.

Kim N.H., Oh C.S., Kim Y.J., Yoon K.B., Ma Y.H., 2011. Comparison of fracture strain based ductile failure simulation with experimental results. International Journal of Pressure Vessels and Piping 88, 434–447.

Kim Y.J., Kim J.S., Cho S.M., Kim Y.J., 2004. 3-D constraint effects on J testing and crack tip constraint in m(t), se(b), se(t) and c(t) specimens: Numerical study. Engineering Fracture Mechanics 71, 1203–1218.

Larrosa N.O and Ainsworth R.A., 2016. Ductile fracture modelling and J-Q fracture mechanics: a constraint based fracture assessment approach Frattura ed Integrita Strutturale, (in press), 2016.

McClintock F., 1968. A criterion for ductile fracture by the growth of holes. Journal of Applied Mechanics. 35, 363–371.

McMeeking R., Parks D., 1979. On criteria for J-dominance of crack-tip fields in large-scale yielding. ASTM STP 668, 175–194.

Meek C., Ainsworth R.A., 2014. Ductile fracture assessment of plates under biaxial loading. American Society of Mechanical Engineers, Pressure Vessels and Piping Division , volume 6A.

Meek C., Ainsworth R.A., 2015. The effects of load biaxiality and plate length on the limit load of a centre-cracked plate. Engineering Fracture Mechanics 147, 306–317.

Milne I., Chell G.G., Worthington, P.J., 1979. The mechanisms of fracture in blunt-notched specimens of a low alloy steel and the effect on failure assessment. Materials Science and Engineering 40, 145–157.

O'Dowd N., Shih C., 1991. Family of crack-tip fields characterized by a triaxiality parameter-I. structure of fields. Journal of the Mechanics and Physics of Solids 39, 989–1015.

Oh C.K., Kim Y.J., Baek J.H., Kim Y.P., Kim W., 2007. A phenomenological model of ductile fracture for api x65 steel. International Journal of Mechanical Sciences 49, 1399–1412.

Oh, C.S., Kim, N.H., Kim, Y.J., Baek J.H., Kim Y.P., Kim W.S., 2011. A finite element ductile failure simulation method using stress-modified fracture strain model. Engineering Fracture Mechanics 78, 124–137.

Parks D., 1977. The virtual crack extension method for nonlinear material behavior. Computer Methods in Applied Mechanics and Engineering 12, 353 – 364.

Pineau A., 2006. Development of the local approach to fracture over the past 25 years: Theory and applications. International Journal of Fracture 138, 139–166.

Rice J., Tracey D., 1969. On the ductile enlargement of voids in triaxial stress fields. Journal of the Mechanics and Physics of Solids 17, 201–217.

Ruggieri C., Dodds R., 1996. A transferability model for brittle fracture including constraint and ductile tearing effects: A probabilistic approach. International Journal of Fracture 79, 309–340.

Shih C., German M., 1981. Requirements for a one parameter characterization of crack tip fields by the HRR singularity. International Journal of Fracture 17, 27–43.

Shih C., Moran B., Nakamura T., 1986. Energy release rate along a three-dimensional crack front in a thermally stressed body. International Journal of Fracture 30, 79–102.

Spink G.M., Worthington P.J., Heald P.T., 1973. The effect of notch acuity on fracture toughness testing. Materials Science and Engineering 11, 113–117.

Yuan H., Brocks W., 1991. On the J-integral concept for elastic-plastic crack extension. Nuclear Engineering and Design 131, 157–173.